Control of syntectonic erosion and sedimentation on kinematic evolution of a multidecollement thrust zone: Analogue modeling of folding in the southern subandean of Bolivia

Romain Darnault, Jean-Paul Callot, Jean-François Ballard, Guillaume Fraisse, Jean-Marie Mengus, Jean-Claude Ringenbach

Control of syntectonic erosion and sedimentation on kinematic evolution of a multidecollement thrust zone: Analogue modeling of folding in the southern subandean of Bolivia..

Romain Darnault[1], Jean-Paul Callot[2], Jean-François Ballard[3], Guillaume Fraisse[4], Jean-Marie Mengus[1], Jean-Claude Ringenbach[3]

1 : IFP Energies nouvelles, 1-4 avenue de Bois Préau, Rueil Malmaison France

2 : LFCR UMR 5150, Université de Pau et des Pays de l'Adour, Avenue de l'Université, 64013, Pau France

3 : Total SA, CSTJF, Avenue Larribau, Pau, France

4 : ENSG, Avenue du Doyen Marcel Roubault, 54501, Vandoeuvre lès Nancy, France

Abstract

Several analogue modeling studies have been conducted during the past fifteen years with the aim to discuss the effects of sedimentation and erosion on Foreland Fold and Thrust Belt, among which a few have analyzed these processes at kilometric scale (Nalpas et al., 1999; Barrier et al., 2002; Pichot and Nalpas, 2009). The influence of syn-deformation sedimentation and erosion on the structural evolution of FFTB has been clearly demonstrated. Here, we propose to go further in this approach by the study of a more complex system with a double decollement level. The natural study case is the Bolivian sub-Andean thrust and fold belt, which present all the required criteria, such as the double decollment level. A set of analogue models performed under a CT-scan have been used to test the influence of several parameters on a fold an thrust belt system, among which: (i) the spatial variation of the sediment input, (ii) the spatial variation of the erosion rate, (iii) the relative distribution of

sedimentation between foreland and hinterland. These experiments led to the following observations:

1. The upper decollement level acts as a decoupling level in case of increased sedimentation rate: it results in the verticalization of the shallower part (above the upper decollement level), while the deeper parts are not impacted;
2. Similarly, the increase of the erosion rate involves the uplift of the deeper part (below the upper decollement level), whereas the shallower parts are not impacted;
3. A high sedimentation rate in the foreland involves an inversion of the vergence followed by a back-thrusting of the shallower part.
4. A high sedimentation rate in the hinterland favors thrust development toward the foreland in the shallower parts.

1. Introduction

Several studies have shown the influence of surface processes on the structural evolution of fold an thrust belt systems, both at the scale of lithosphere and of thrust belt system, based on analogue modelling (Cobbold et al., 1993; Malavieille et al., 1993; Baby et al., 1995; Storti et McClay, 1995; Tondji Biyo, 1995; Mugnier et al., 1997; Chemenda et al., 2000; Diraison et al., 2000; Koyi et al., 2000; Leturmy et al., 2000; Nieuwland et al., 2000; Storti et al., 2000; Bonini, 2001, Smit et al., 2003). Among them, several studies already tried to analyze the relative importance of controlling parameters such as erosion, sedimentation, decollement coupling efficiency and dip, and ratio between ductile and brittle layer at the scale of unitary compressive structures (Tondji Biyo, 1995; Nalpas et al., 1999; Casas et al., 2001; Barrier et al., 2002; Nalpas et al., 2003; Gestain et al., 2004; Pichot and Nalpas., 2009; Vidal-Royo et al., 2011; Barrier et al., 2013; Driehaus et al., 2014). In particular, these studies demonstrated the fundamental role played both by syn-kinematic sedimentation and erosion on the

evolution of geological structures during compression. However, single decollement system, if already quite well understood, are quite rare: most of the time, the presence of several decollement levels within the stratigraphic pile tends to isolate several systems that can or not be decoupled from each other, depending of various parameters among which external factors like sedimentation and/or erosion, deformation rate, a strong rheological contrast (e.g. Couzens-Schultz et al., 2002). Only a few studies focused on the impact of these parameters if the mechanical pile includes several prekinematic decollement level, namely two (e.g. Couzens-Schultz et al., 2003; Pichot et al., 2009) or three (e.g. Driehaus et al., 2014), which is nevertheless a quite common natural case, observed in the Zagros fold-and-thrust belt (Verges et al., 2011), the bolivian subandean belt (Baby et al., 1999; Labaume and Moretti, 2001), or else the Rocky Mountains (e.g. Lebel et al. 1996) for instances.

They showed that deformation is strongly dependent on sedimentation rate: (i) the structures propagate forward with an overall asymmetric shape if the sedimentation is slower than the uplift velocity, (ii) the structures grow vertically and can present vergence inversion at the surface if the sedimentation rate is similar to the uplift velocity, and (iii) the structures grow vertically with a double vergence at the surface and at depth if the sedimentation rate is higher than the uplift velocity (Barrier et al., 2013; Driehaus et al., 2014); eventually, if the sedimentation rate is much higher than the tectonic uplift rate, a symmetrical pop-up, independent from the internal mechanical stratification, forms. These experiments showed that the kinematic scenario of the fold development appears to be the first order element that discriminate the various interferences between sedimentation and fold growth.

Following Driehaus et al. (2014), the present study aims at the characterization of the fold kinematic scenario analysis, in order to properly constrain the relative importance of internal factors such as rheological stratigraphy and kinematic boundaries, upon external forcing such as sedimentation and erosion. To fulfill that goal, we propose a set of analogue models

imaged with an X-ray CT scanner (Colletta et al., 1991), which allows for a non destructive 3D, time repeated acquisition of the internal model geometry. It thus offers access to the kinematic evolution of the geometries. These experiments aim at completing the previous studies set in 2D, and to characterize both in 3D and through time the influence of external factors (sedimentation and erosion) on a decoupled system known in the literature: the sub Andean compressive system. This geological case is also a strategic petroleum basin representing crucial economic issues that depends of the geological knowledge of the area. The understanding of the 3D structural evolution is thus crucial for this area. However, due to the geometric complexity of such geological systems, seismic imagery can't mostly provide well-defined images of the deeper part of such folded systems (Figure 1). It is thus crucial to understand the evolution of the superimposed structures of these areas to provide pertinent interpretation and assessments of eventual HC resources. In a first approximation, analogue modelling can bring elements to better understand these complex structural domains and some relationships between shallow and deep-seated structures.

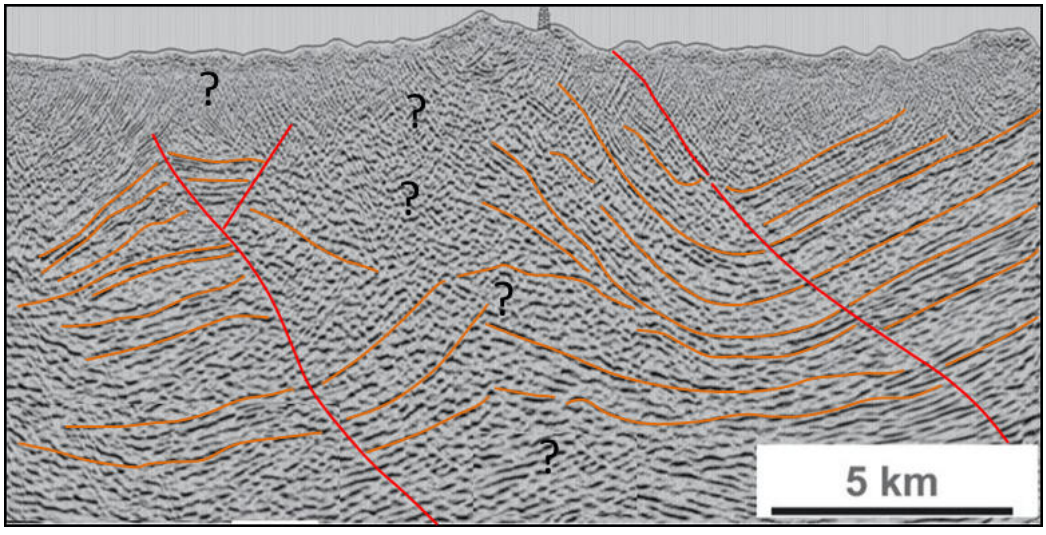

Figure 1: Example of seismic profile in sub-Andean zone. The geometrical complexity doesn't allow a well-defined seismic imagery.

2. Geological and geographical settings

The southern Sub-Andean Zone (SAZ), of Bolivia, is a Neogene foreland fold and thrust belt., which constitutes the Eastern border of Andes (Figure 2a).

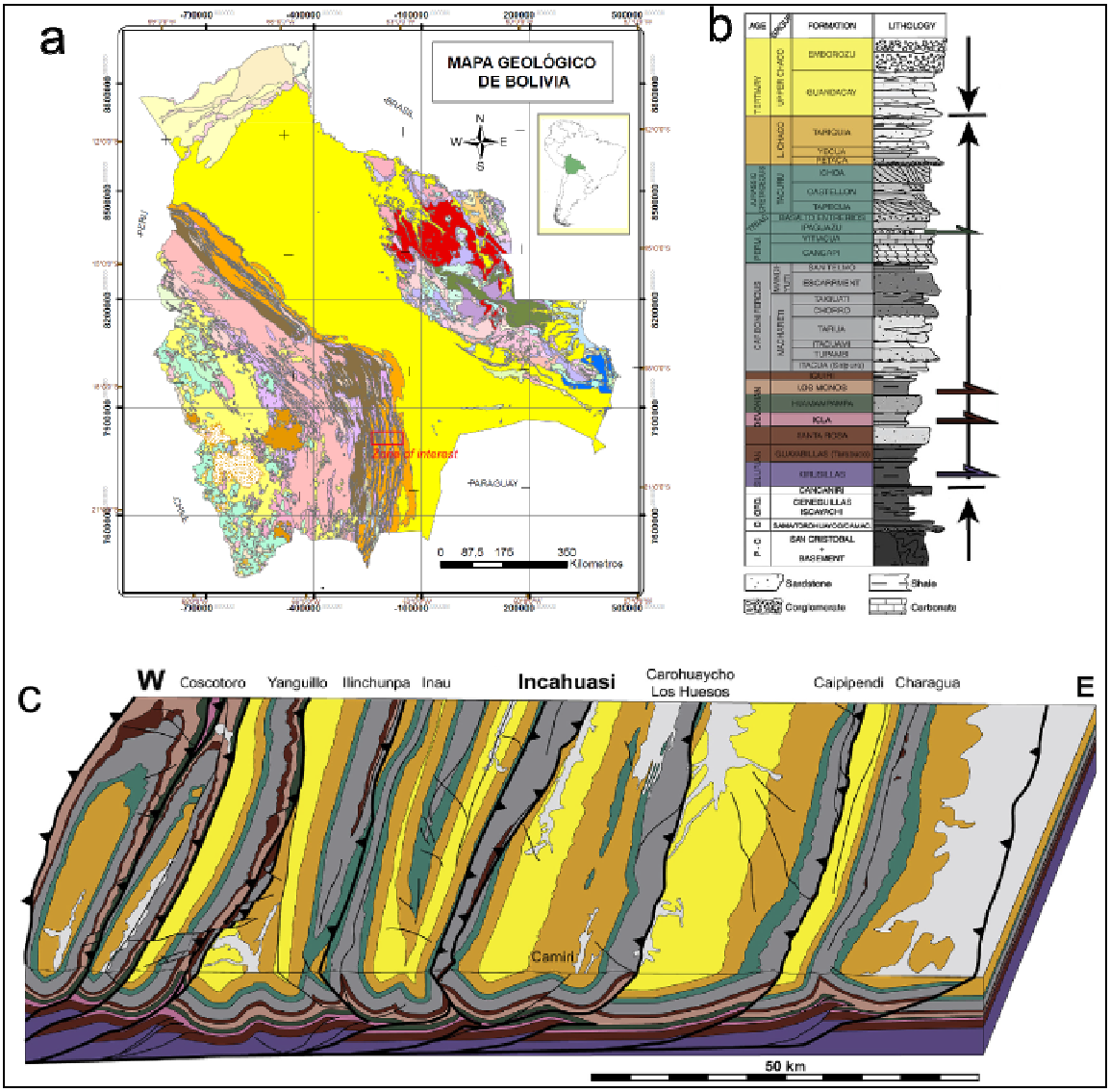

Figure 2: a. Localisation of the study area. The rectangle indicates the modelled area. **b.** Lithostratigraphic scale of the modelled area. c. Geological cross section of the modelled area (Driehaus et al., 2014.

2.1 Sedimentary sequence and mechanical stratigraphy

The SAZ stratigraphy is formed by a thick, mainly siliciclastic, Paleozoic to Quaternary succession developed above the Precambrian basement (Sempere, 1995; Uba et al., 2005; 2006; Figure 2b). The lower part of the Paleozoic succession is marine, with about 4 km of Silurian to Devonian levels including a considerable thickness of marine shales forming the

major decoupling levels (namely the Kirusillas, Icla and Los Monos formations) alternating with sandstones levels (Tarabuco, Santa Rosa, Huamampampa and Iquiri formations; Moretti et al., 2002). The Subandean Carboniferous-Early Permian cycle is characterized by the deposition of marine to glacial sands and diamictites, indicating a periglacial environment. The carboniferous deposits (Machareti and Mandiyuti groups) have a total thickness of about 2 km, composed mainly of sandstones (Tupambi, Chorro and Escarpment Fms).

The overlying sediments are mainly continental, with few hundred meters of Lower Permian fluvial-eolian sandstones (Cangapi Formation), a few tens of meters of evaporitic Upper Permian carbonates (Vitiacua Formations), Lower Triassic anhydrite/gypsum and about 1 km of upper Triassic to Cretaceous fluvial and eolian sandstones (Tacuru Gr.). The Yecua Formation presents lacustrine facies with locally marine influences (Marshall et al., 1993). Above these units, the foreland sequences of Lower and Upper Chaco are composed of distal clastic facies of fluvial plains (with anastomosed fluvial channels) evolving to more proximal facies characterized by conglomeratic beds (Moretti et al., 2002).

2.2 Structural setting

The SAZ is a Neogene, east-verging, thrust system that constitutes the Eastern border of Andes with a width of about 150 km. The main thrusts have an average spacing of 15 km with a displacement of several km (Figure 2c). This thrust system involves the Upper Silurian to Quaternary succession, which is about 10 km thick. The main basal decollement level has been defined as located in the Silurian shales (Baby et al., 1993; Colletta et al., 1999), while secondary decollements are located in the Middle Devonian (Icla and Los Monos Formations) and locally in the Carboniferous diamictites (Moretti et al., 2002). Note that Devonian shaly formations are also the source-rocks of the petroleum systems, the maturation of which could have influenced the decollement localization and timing of activity (e.g. Cobbold et al. 2009).

Folds and thrusts geometries are mainly controlled by lithology and by these decollement levels. Among the sub-andean structure, the Incahuasi trend has the particularity to be west verging, and offset by at least 1 km to the East (Driehaus et al., 2014). The shallow part of the fold has a west vergence, while the other folds are oriented toward the East (Figure 2c). Driehaus et al. (2014) explained this difference of vergence by the effect of the sediment rate variation.

The development of the structural system started during the Late Oligocene (27 Ma ago) and implies a general eastward propagation of the thrust system (Baby et al., 1993; Gubbels et al., 1993; Moretti et al., 1996), although deformation in the Eastern Cordillera may have started earlier (Buttler et al., 1995).

Shortening in the sub-Andean zone is relatively recent and occurred mainly between the Upper Miocene (6 Ma from apatite fission track and tuff intercalations; Moretti et al., 1996) and present (Gubbels et al., 1993; Labaume et al., 2001), resulting in the uplift and erosion of the anticlines.

3. Experimental procedure

3.1. Experimental set-up:

Analogue models were built in a 70 x 40 cm wood deformation box (Figure 3). The box presents two free sides and two walls: the first one is fixed and the second one is mobile and linked to a stepper motor allowing shortening. For this set of experiments, we choose to focus on the modeling of one typical fold structure representing the evolution of the Incahuasi fold. For this reason, a moving carpet is attached to the mobile wall generating a velocity discontinuity in the middle of the box (Figure 3), which localizes the initiation of the structure on the velocity discontinuity location that represents either a deep-seated fault or else the tip line of the basal decollement level. In addition, this discontinuity allows studying the

158 evolution of a single fold avoiding the parasitic influence of neighboring structures. All the
159 experiments have been performed under an X-ray tomographer for a 3D imagery. The use of
160 this technology allows a non-destructive 3D-image acquisition at regular stages of evolution
161 of the model, with the possibility to reconstruct 3D geometries at different deformation stages
162 (Colletta et al., 1991).

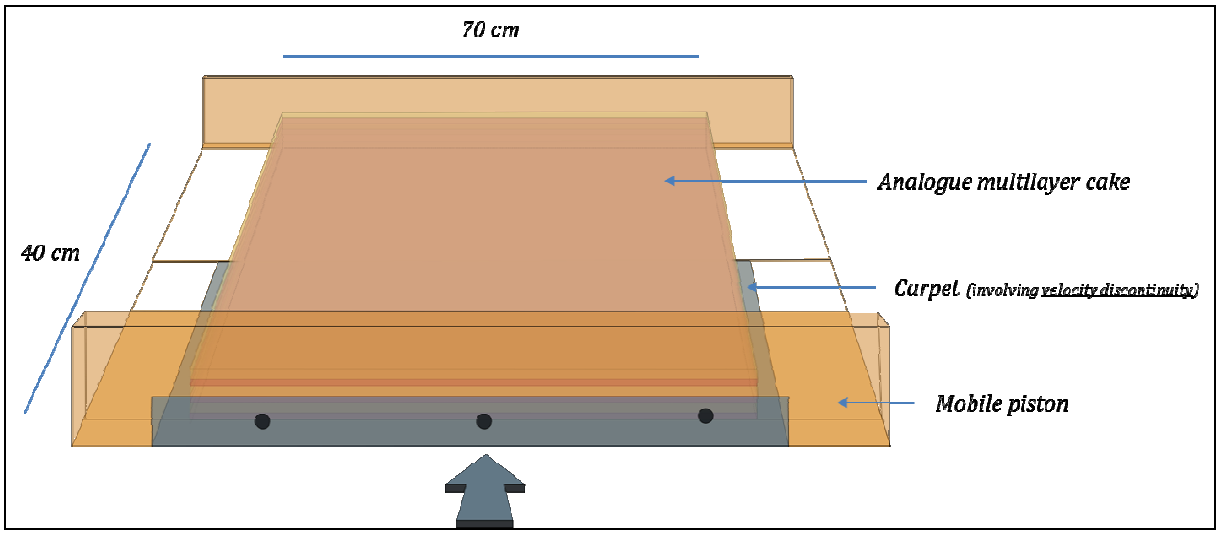

163

164 **Figure 3:** Illustration of the deformation box used for analogue model. The mobile wall is animated by a stepper
165 motor, which is set up to generate a constant shortening. A velocity discontinuity is generated by the carpet,
166 which is linked to the mobile wall.
167

168 The models were scaled for length, viscosity and time, following the basic principles,
169 discussed by Hubbert (1937) and Ramberg (1981). The length ratio between models and
170 natural examples is 10^{-5} (1 cm in the model represents 1 km in the nature). The viscosity ratio
171 is of the order of 2.10^{-15} considering a 10^{16} Pa.s as a mean viscosity for mobile shales. The
172 time ratio equals thus to 1.10^{-10}. This analogue modeling protocol does not allow taking into
173 account some geological parameters such temperature gradient or rheological changes, among
174 others.

175

176 **3.2. Analogue material:**

177 Three types of analogue material were used to simulate different rheological behaviors:

- dry granular materials to simulate brittle sedimentary rocks, which obey to a Mohr-Coulomb failure criterion;
- viscous Newtonian material to simulate ductile rocks such as shales, acting as decollement levels;
- a mixture of viscous material (silicone putty) with granular material (sand) in order to increase the viscosity of this layer and allowing a greater coupling between ductile and brittle layer (see Callot et al., 2012 for the material scaling).

Sedimentary brittle rocks were simulated using sand, pyrex and microbeads with a grain size of 100 μm. Sand has a negligible cohesion, an angle of internal friction of 30° and a density close to 1600 kg/m^3 (depending on sieving procedures). Pyrex has approximately the same brittle behavior than sand but a contrasted radiological density, which differentiates them on tomographic images. Microbeads have a similar brittle behavior but an angle of internal friction of 20° (Schreurs et al., 2006), which promotes low angle thrusting behavior in the model. Layers of silicon putty (SGM36) simulate the ductile behavior of weak layers, corresponding to the decollement levels in the sub-Andean case. Silicone behaves as a Newtonian fluid, with a density close to 1 g.cm^{-3} and a viscosity of 2.5.10^4 Pa.s at room temperature and strain rates below 3.10^{-3}s^{-1}.

3.3. Experimental design

Each model is based on a single rheological and stratigraphic pile, defined by Driehaus et al. (2014) (Figure 4): A 6 mm thick silicone layer models the main basal Silurian decollement level. The Late Silurian to Devonian units (Tarabuco formation to Huamampampa formation) are modelled by a 10mm-thick alternance of 3mm tick sand and microbeads. The decollement of the Middle Devonian (Los Monos Formation) is represented by a 5-7 mm thick silicone layer inside this unit. The top of the sequence corresponding to Carboniferous to Cretaceous

series is modeled by two couples of sand and pyrex layers (respectively 10 and 12 mm thick) separated by a 3 mm thick mixture of sand/silicone (50%/50% weight proportion). A thin layer, less than 1 mm thick, of pumice powder marks the boundary between pre-kinematic sedimentation and syn-kinematic sedimentation. A shortening rate between 1,5 and 1,7 cm/h is applied. During the experiment, syn-kinematic sedimentation is performed by sprinkling sand ontop of the model. Syn-kinematic sedimentation is composed of alternating sand and pyrex layers. Amount of sedimentation and erosion are determined by ratios allowing the characterization of each model, as explained in Driehaus et al. (2014):

- The “R” ratio represents the amount of sedimentation with R = Velocity of sedimentation / Velocity of uplift.
- The “E” ratio represents the amount of erosion with E = Velocity of erosion / Velocity of uplift.

The X-ray tomographer allows the observation of the experiment state in real time, which is helpful for the estimation of the amounts of sediments that have to be added or removed.

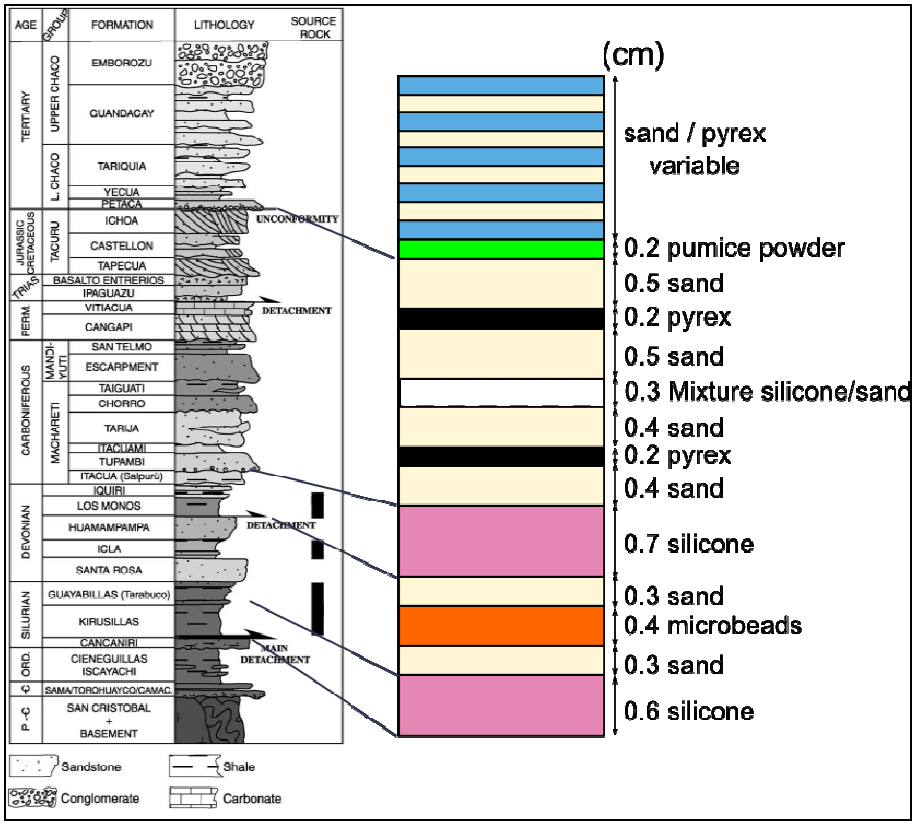

Figure 4: Analogue rheology used for experiments. The stratigraphic column is from Moretti et al.(1996).

3.4. Reproducibility of the results.

Numerous experiments have been performed since the initial presentation of the use of X-Ray tomography technology for a sandbox model (Colletta et al., 1991). Their reproducibility depends on the building precision of the layered sequence. The influence of subtle, wavy undulations (relief less than 0.5 mm) that may occur in the silicone layer is always controlled with the scanner imagery to be sure that the model is homogenous. If the cylindricity of the structures is preserved above non-cylindrical irregularities, their effect is negligible and the result considered reliable. This test is easily performed as (1) the deformation box is longer along the strike direction than along the shortening direction, and (2) as the X-Ray scanner gives a continuous 3D view with a spatial resolution better than 0.3 mm.

4. Analogue model results

4.1 Preliminary calibration experiment

A set of analogue experiments has been performed for this study to observe the spatial influences (in 3D) of (i) sedimentation, (ii) erosion, (iii) localized sedimentation and (iv) rheology, on syn-kinematic evolution of a Sub-Andean mono-structure type. Before realizing this set of experiments, a preliminary test was been performed to scale and calibrate experimental parameters with respect to already published analogue models (Driehaus et al., 2014, Figure 5).

The lower structure behaves as a duplex for six and eight percent of shortening and wraps on itself at higher shortening amount (24%). This geometry fit with the exploration data available for the analogue natural case (e.g. Driehaus et al., 2014).

The upper structure behaves as an asymmetric fold, which as a fish-tail structure, the lower thrust grading upward as a flat in the upper decollement level, triggering a second, anthitetic thrust ramp in the upper pre-tectonic and syn-tectonic sequences. (Figure 5, compression of 6% and 8%). For higher shortening amount (24%), the fold vergence changes again, developing a thrust, synthetic to the lowermost one, and rooted along the fold limb in the upper decollement level. This thrust decapitates the tight fold's head. These results are in close agreement with the experiments of Driehaus et al (2014) and their 2D analyses.

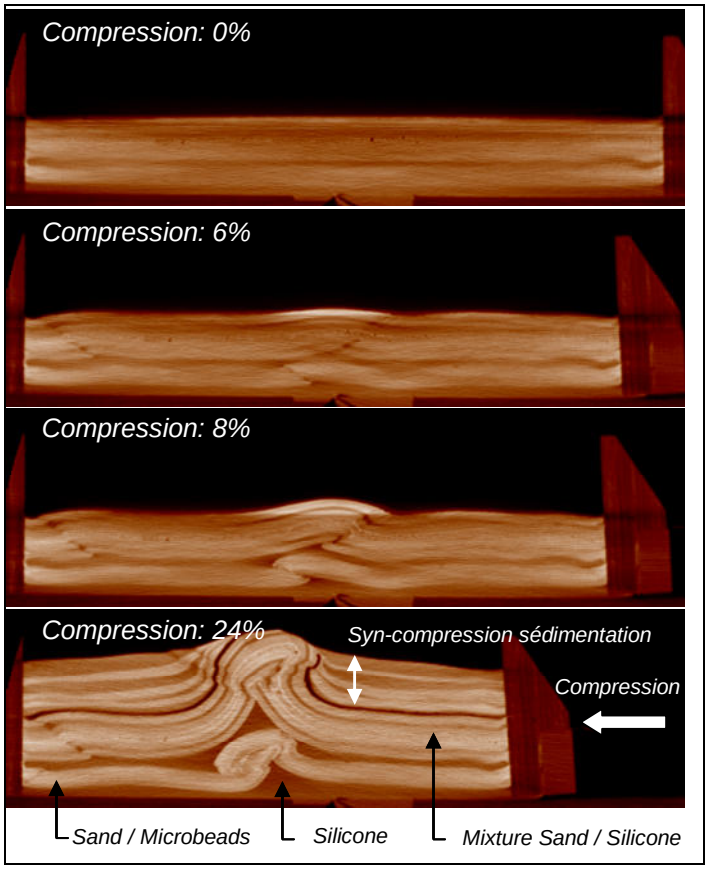

Figure 5: Results of the first experiment realized to test the mechanical behaviour of the model with scaled parameter (rate of compression is 1,7 cm/h; choice of material and thickness of layers: **Figure 4**). For this experiment, syn-kinematics sedimentation and erosion have been established following the results obtained by Pichot et Nalpas, 2009: For sedimentation, R=1/2. For erosion, E=1/4 (see section 3.3 for more details of R and E ratios).

4.2. Influence of sedimentation

The aim of this experiment was to test the influence in 3D of sedimentation on the development of a folded structure.

4.2.1. Experimental set up

This experiment was set up using the rheology established previously (Figure 4) and the same deformation rate. No erosion was performed for this experiment. Differential sedimentation was applied during shortening along the deformation box in order to obtain a R ratio ranging from ½ to 1 along strike of the growing structure.

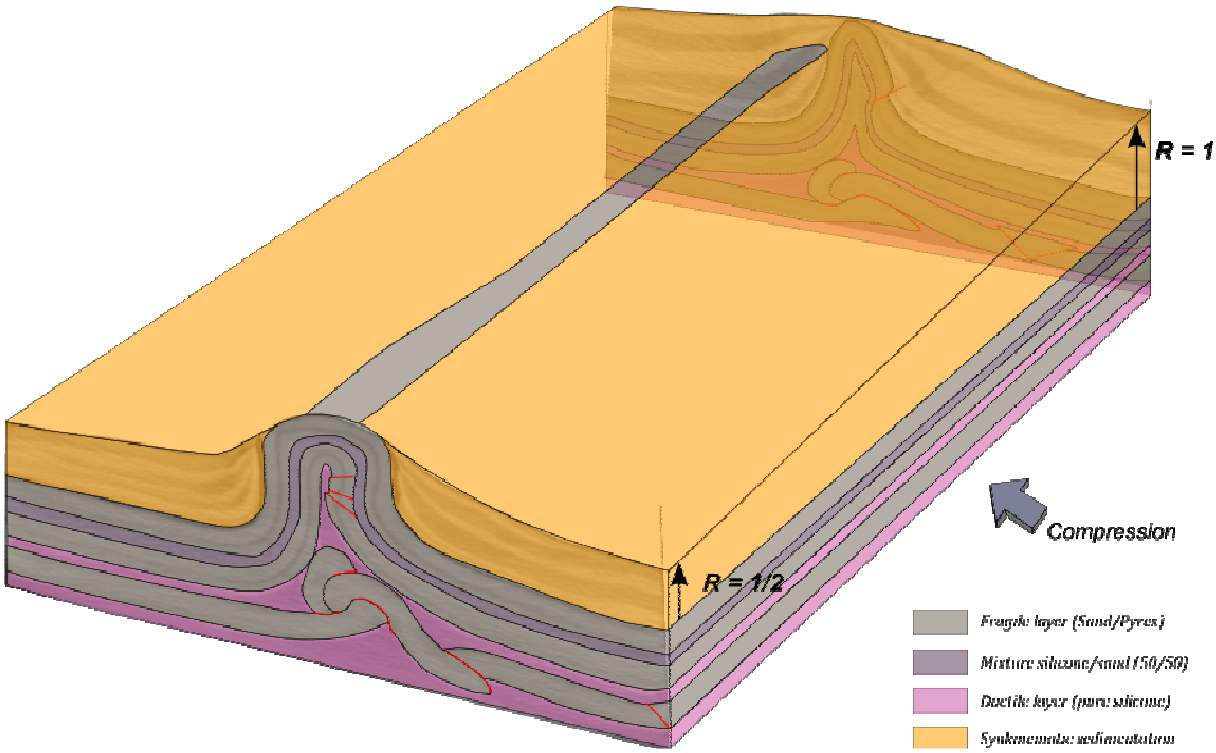

Figure 6: 3D sketch of the model performed to study the syn-kinematic impact of sedimentation in 3D. The sedimentation rate vary along the deformation box, from R=1 to R=½. No erosion has been performed and a compression rate of 1,7 cm/h was applied. Red sticks show faults generate during the deformation.

4.2.2. Impact of the sedimentation rate distribution

The topography is directly impacted by the increase of sedimentation rate during the compression (Figure 7 and Figure 8): Raise up of the topography follows high sedimentation rate (R=1, Figure 8). In this case, the syn-kinematic sedimentation progressively pinches the folded structure, which rises vertically in response to shortening, and is less faulted than in the lower sedimentation case (compare figures 7C and D). This modification of topography involves also a variation of the vergence for shallow structures (Figure 7C and Figure 9). In

case of high sedimentation compared to tectonic uplift, the shallow structure is much more symmetric and evolves form the fish-tail backthrust to a large scale pop-up.

The depth structures appear not to be impacted by the syn-deformation sedimentation (Figure 7C and D). Their geometries stand relatively flat all along the deformation box without vergence variation nor topographical modification.

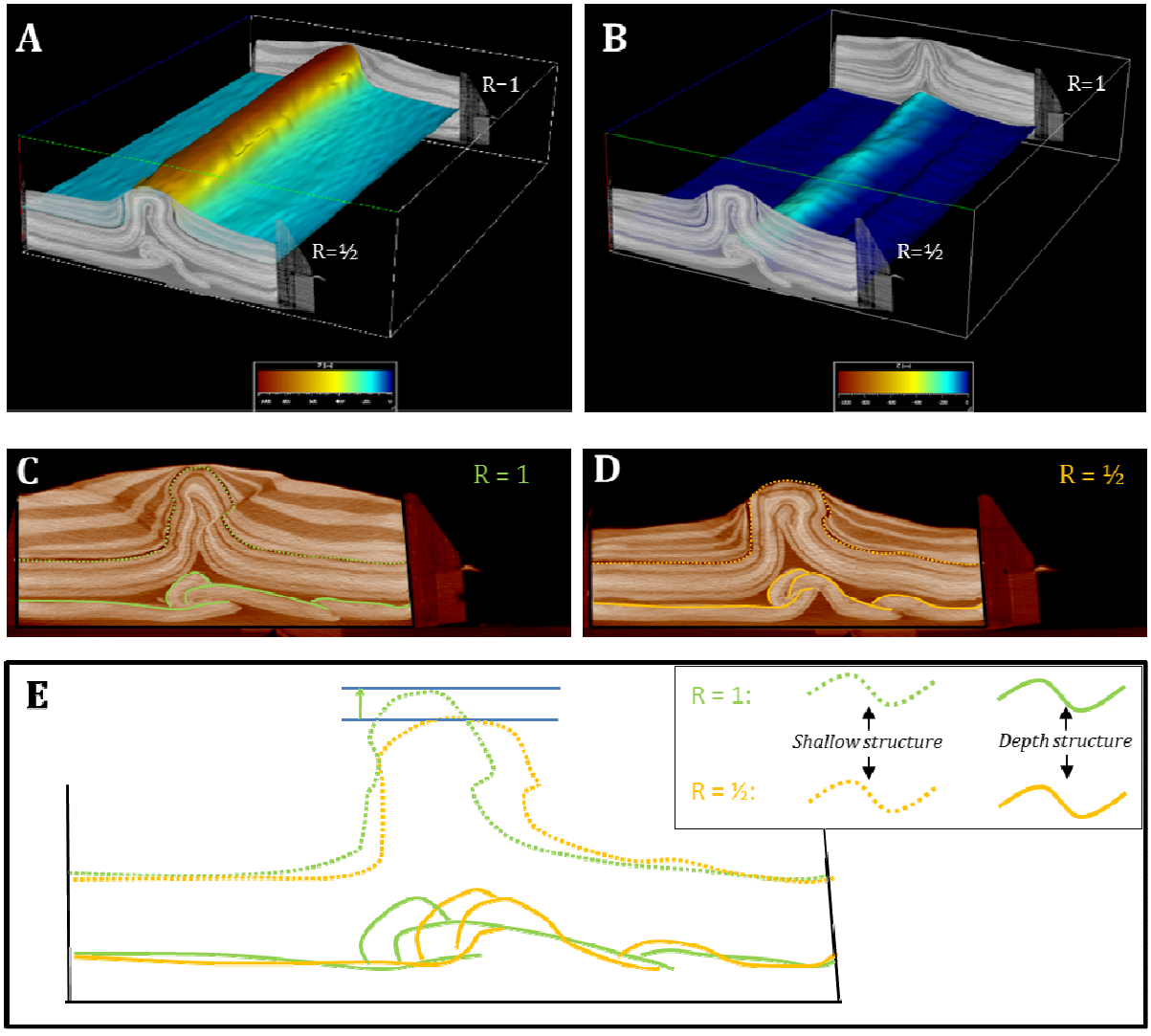

Figure 7 : A. 3D bloc showing two inline sections bordering the elevation map of the shallow structure's top. It shows the uplift of the shallow structure for a high sedimentation rate (R=1). **B.** 3D bloc showing two inline sections bordering the elevation map of the depth structure's top. It shows the cylindricity of the depth structure, which is not impacted by the variation of the sedimentation rate. **C and D**. are Inlines corresponding to the high sedimentation rate (R=1) and low sedimentation rate (R=½), respectively. **E.** Superposition of the shallows (dashed lines) and depth horizons for a high sedimentation rate (in green) and a low sedimentation rate (in yellow); right part is the legend. It shows the delta between the elevation of the shallow structures subjected to a high sedimentation rate and the shallow structure subjected to a low sedimentation rate. In contrast, there is no delta for the depth structures.

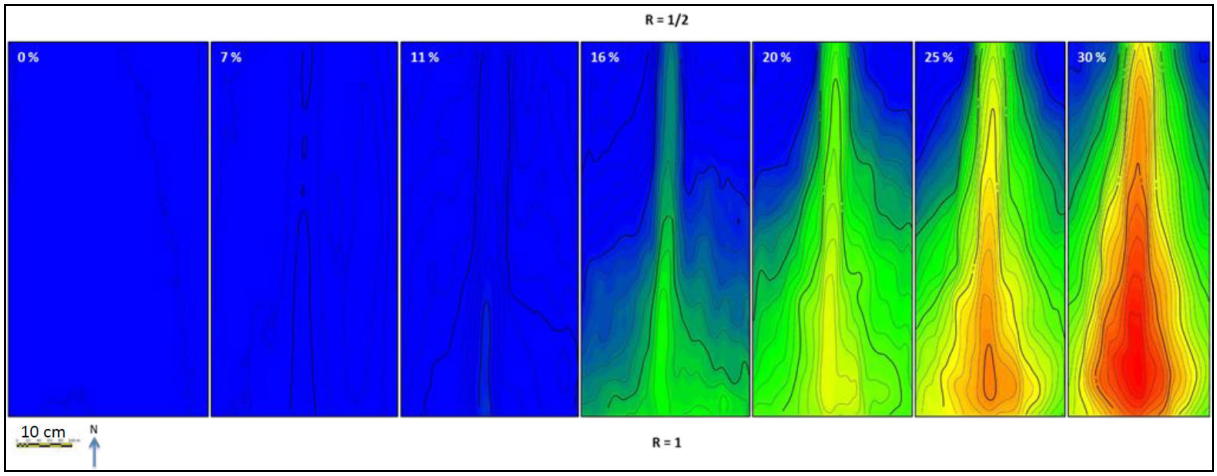

Figure 8: Map of the shallow structure (top of the model) illustrating the impact of the sedimentation on the model's topography with the increase of compression. Percentage in white corresponds to the amount of shortening. R ratio end members are located at both ends of the maps. The colour scale (from blue (0mm of elevation) and red (75 mm of elevation)) represents relative topography: It represents a different elevation of 9 mm between R=1 side and R=½ side.

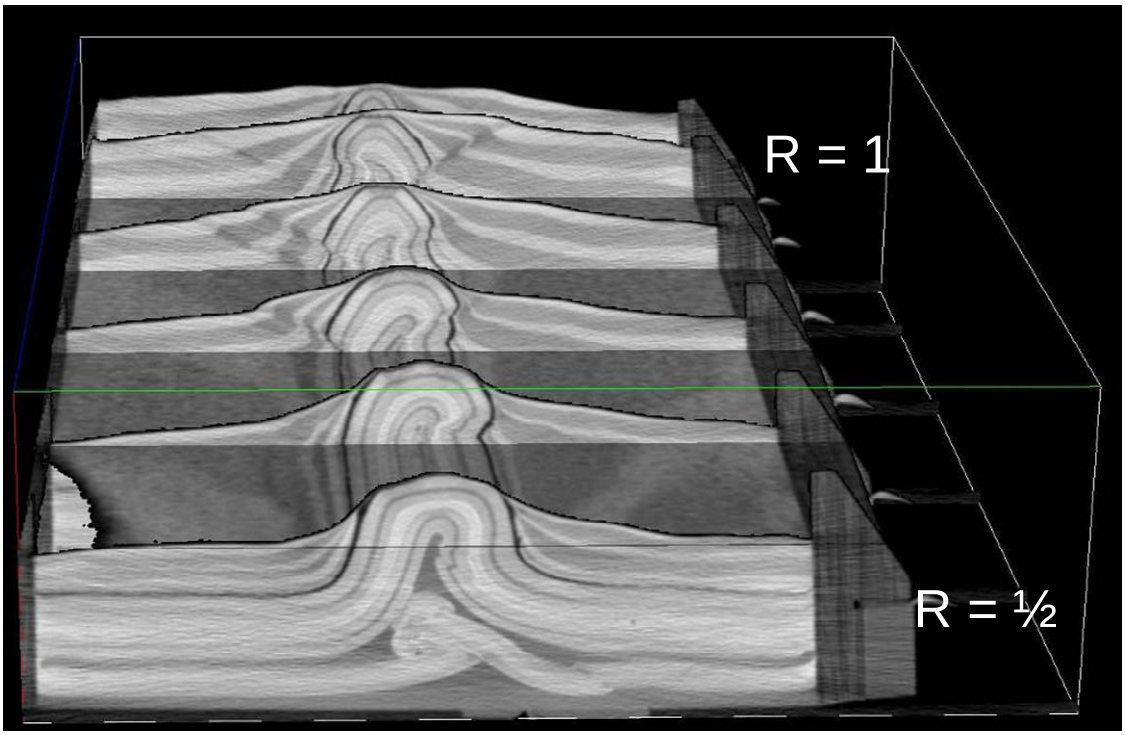

Figure 9: 3D view of the model showing the modification of shallow structure vergences: The background shallow structures (R=1) are verticals with a low left vergence, while foreground shallow structures (R=½) have a right vergence.

These observations, which are in agreement with the results of Driehaus et al (2014) show that the system is highly decoupled because of (i) the ductile inter-bedded layer but also (ii)

by the syn-kinematic sedimentation. This 3D analysis brings new elements about the geometrical variation in space induced by syn-compression sedimentation. This decoupling is able to involve a vertical misfit between apexes of shallow and deep structures, despite a general cylindrical aspect of the map view. Sedimentation impacts the shallow structure evolution and constraints the deeper structure development, which appears more confined at depth in the case of high sedimentation: high sedimentation forces the upright development of the fold, and limits the elevation of the kink folds responsible for the fold development at depth. The lower structure is thus pushed downward. On the contrary, for low sedimentation rate, the propagation of the fish tail, and the formation of the second, synthetic, thrust affecting the backlimb of the shallow fold, allows for a vertical growth of the deeper structure below the upper ramp (figures 7C and 7D).

4.3. Erosion

The aim of this experiment was to test the influence of the 3D distribution of erosion on the development of the folded structure.

4.3.1 Experimental setup

This experiment was set up using the rheology established previously (Figure 4) and the same deformation rate (1,7 cm/h). We apply a constant sedimentation rate to reach R = ½ over the entire deformed model. Differential syn-compression erosion along strike of the deformation box was applied to obtain a E ratio varying linearly from 0 to ½ (Figure 10).

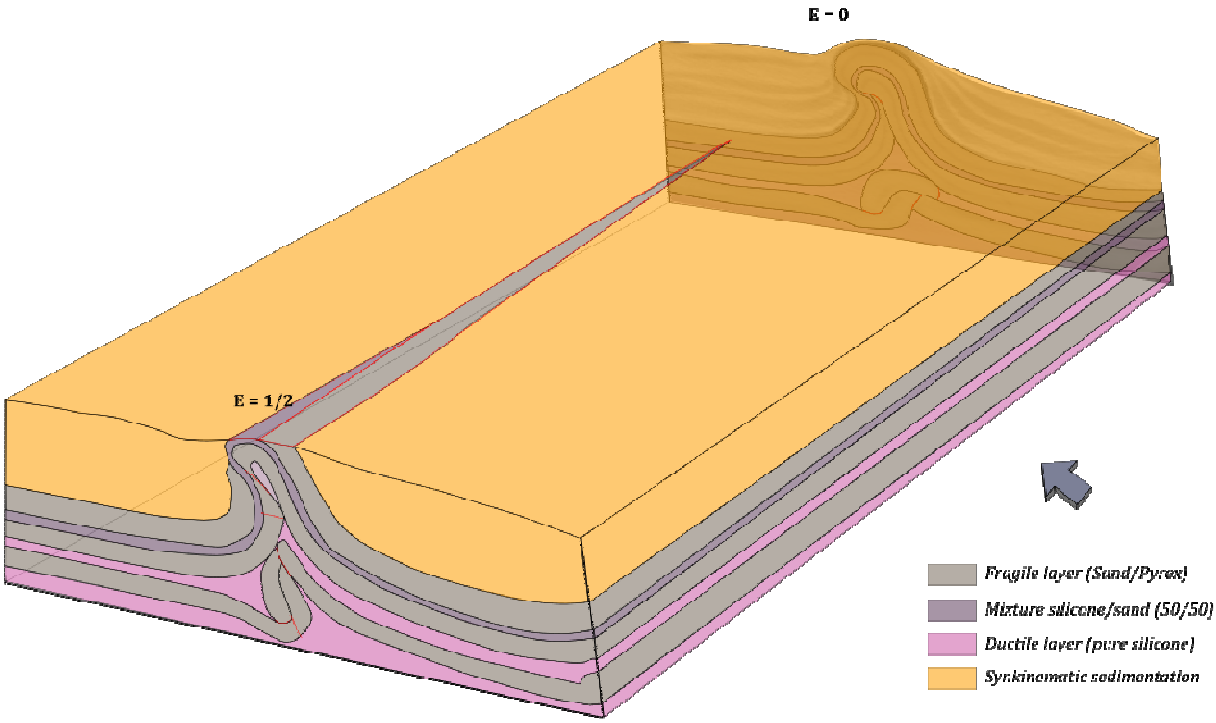

Figure 10 : 3D sketch of the model performed to study the syn-kinematic impact of erosion in 3D. The sedimentation rate is constant along all along the model (R=½), while the erosion vary linearly along the deformation box, from E=½ to E=0. A compression rate of 1,7 cm/h was applied (thick arrow). Red sticks show faults generate during the deformation.

4.3.2 Observations of differences between low and high erosion rate

Several elements can be observed on Figure 11:

- Geometries of shallow structures are poorly impacted by erosion; these structures are principally controlled by compression and sedimentation rate as shown in previous sections. Neither vergences nor topography appear impacted by the variation of erosion rate on shallow structures, apart from the direct effect of erosion. Nevertheless, the steep fold limb appears steeper and more folded if associated to erosion.

- Geometries of deep structures are strongly impacted by erosion. Topography of the apex of depth fold rise when erosion is high (E=½) (Figure 11C and Figure 12) and stands relatively flat when erosion is null (Figure 11D and E, and Figure 12).

The most impressive modification of the model behaviour, related to the increase of erosion with respect to tectonic topography, is the strong and localized uplift of the lowermost

structure. Contrarily to the previous model (figure 7) in which the upper fold kinks were fixed in space, enhanced unloading due to erosion allows for a vertical migration of the upper fold kinks, and thus for the space creation and the uplift of the lower structure.

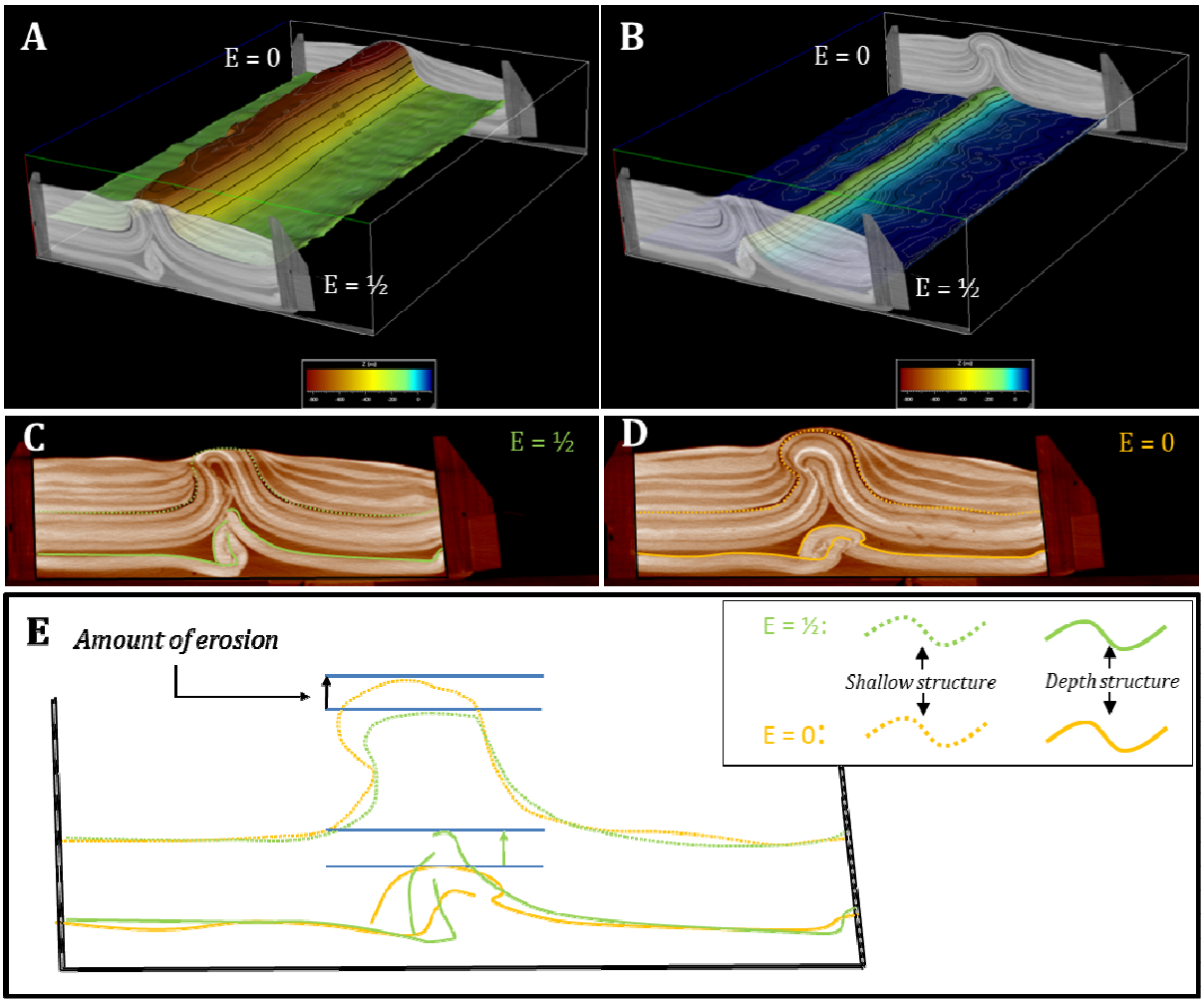

Figure 11: A. 3D bloc showing two inline sections bordering the elevation map of the shallow structure's top. The shallow structure is not affected by syn-deformation erosion and is cylindrical all along the deformation box. **B.** 3D bloc showing two inline sections bordering the elevation map of the depth structure's top. The map shows an uplift of the depth structure in the high erosion part. **C and D**. Inlines corresponding to the high erosion rate (E=½) and no erosion (E=0), respectively. **E.** Superposition of the shallows (dashed lines) and depth horizons for a high erosion rate (in green) and a low erosion rate (in yellow). It show the delta between the elevation of the depth structures subjected to a high erosion rate and the depth structures not affected by erosion. This delta is also present for the shallow structures and represents the amount of erosion of the surface

On one hand, the interbedded layer of silicone generates a decoupling between shallow and deep structures. On the other hand, a high syn-kinematic erosion rate leads to a different behaviour between deep and shallow structures. The decoupling between deep and shallow structures is thus magnified by syn-kinematic erosion,

which involves a lateral misfit between apexes of shallow and deep structures (Figure 13). This misfit could have crucial implications in surface locations and trajectories of exploration and production wells in such area..

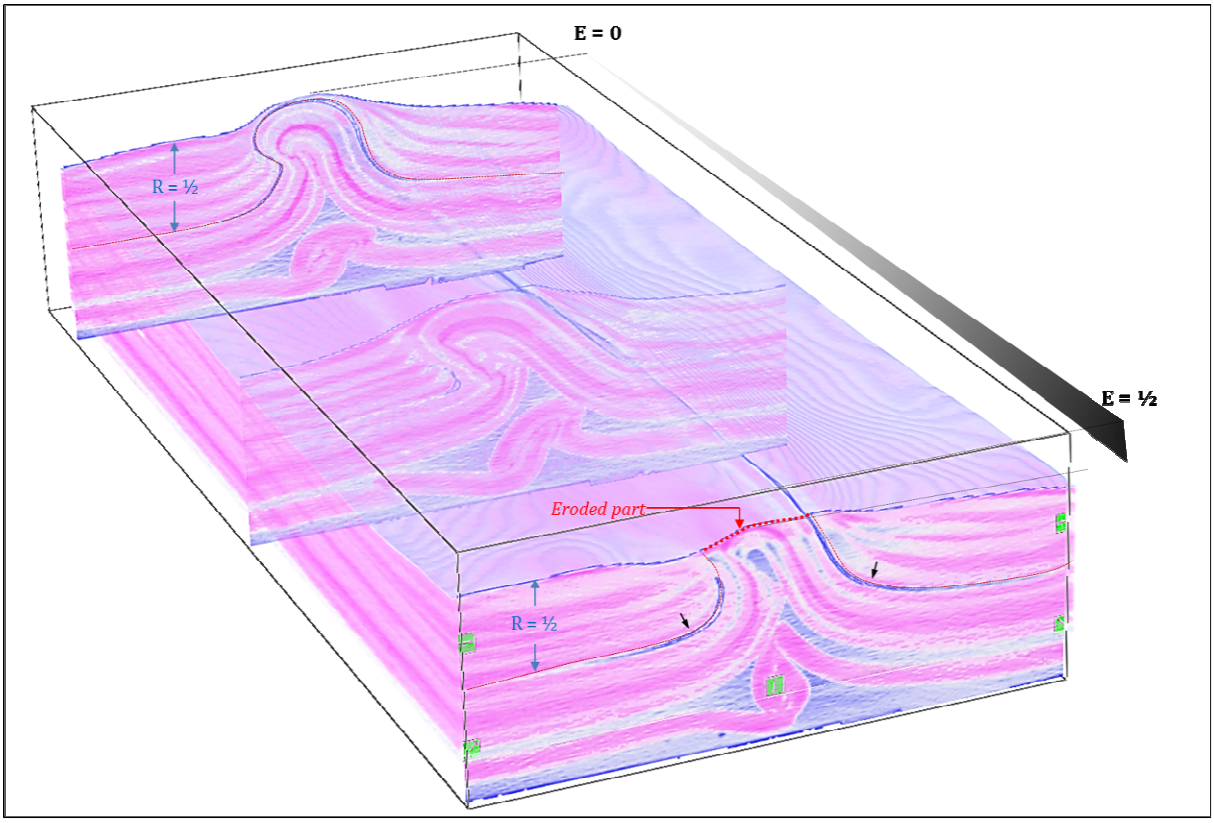

Figure 12 : 3D view of the model performed to study the syn-kinematic impact of erosion. Sedimentation rate is constant along the box (R = ½; blue aorrow) and erosion vary linearly along the deformation box from E=0 to E=½. Black arrows show the thin pumice powder level in blue (less than 1mm), which marks the beginning of syn-kinematic sedimentation.

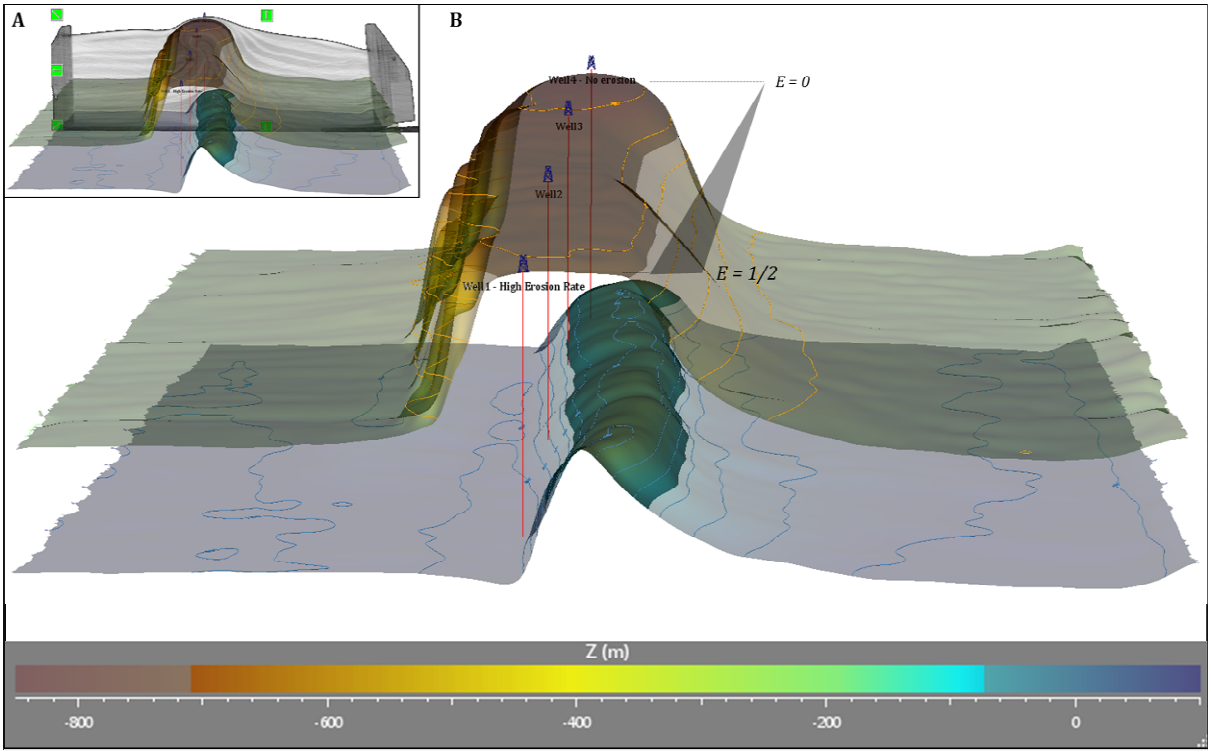

Figure 13: Maps of the two main superimposed folded structures in 3D. Erosion rate increases from background to foreground. Vertical lines (in red) represent virtual vertical well from the apex of topography to deep structures. High erosion rate leads to a lateral misfit between shallow and deep structures.

4.4 Localized sedimentation

Two experiments with sedimentation localized either in the hinterland (figure 14A), or in the foreland (figure 14B) respectively, have been performed. The aim is to observe the evolution of two superimposed structures with an interbedded decollement layer separating two domains (hinterland and foreland) with different sedimentation rate for each one.

4.4.1 Experimental setup

We used the rheology established previously (Figure 4) and the same deformation rate. In the first experiment, sedimentation ratio R was equal to ½ in the hinterland and ¼ in the foreland, while R was equal to ¼ in the hinterland and ½ in the foreland for the second experiment. For each experiment, erosion "E" varied from 0 to ¼ along the deformation box.

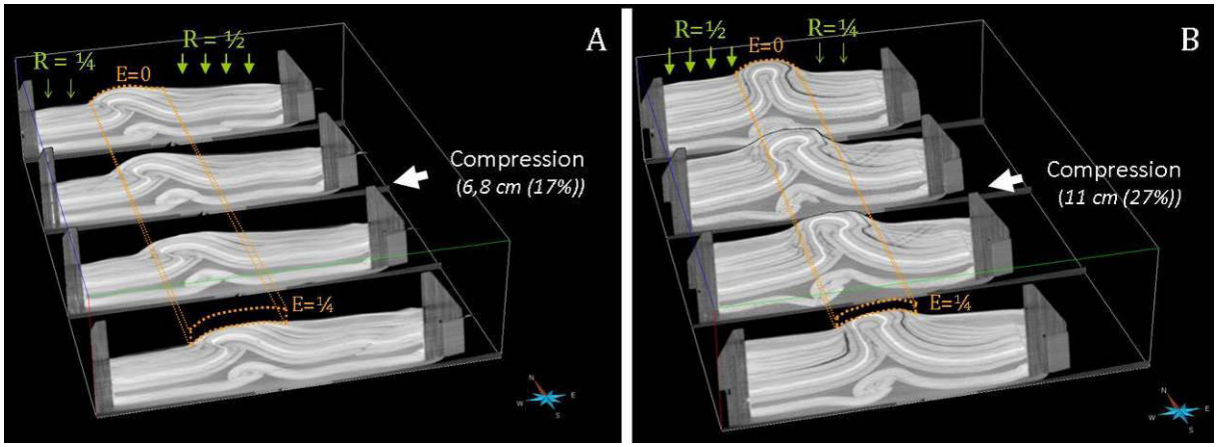

Figure 14: 3D views of two models with different sedimentation rate for hinterland and foreland domains. A. Sedimentation is more important in the hinterland (R = ½ in hinterland vs R = ¼ in foreland). B. Sedimentation is more important in the foreland (R = ¼ in hinterland vs R = ½ in forland). For each experiment, erosion "E" varies linearly from 0 to ¼ along the deformation box.

4.4.2 Results of localized sedimentation experiment

Figure 14 shows two models of two superimposed structures in a system subject to shortening. Some differences can be noticed in first order :

- The deep structures of the two models are quite similar. The thrust, verging toward the foreland is relatively flat in both models. A small uplift of the structure is observable when erosion E is equal to ¼. No significant differences can be attributed to sedimentation distribution for the deep structure evolution.
- The shallows structures of the two models are very different. Figure 14A shows a relatively flat folded structure developped ontop of a thrust ramp breaching the early forelimb, and flattening while propagating upward, verging toward the foreland. On the contrary, Figure 14B displays a tight folded structure, similar to the previous experiments, verging toward the hinterland.

In both cases, there is no significant longitudinal variations along the box.

These observations are concordant with previous models: two superimposed structures in a compressional system with two decollement levels are strongly controlled by the external sedimentation and erosion factors. Depth structures are impacted by syn-kinematic erosion,

while shallow structures are strongly influenced by syn-kinematic sedimentation. The classic foreland ward propagation of fold and thrust is as expected strongly modified when the sedimentation along its front is consequent, whereas sedimentation at the rear only promotes a long-lived activity of the thrust. The absence of foreland sedimentation is the key factor to avoid the change of structure and tightening of the upper fold.

5. Discussion

New elements have been brought by the set of experiments performed for this study. We have been able to (i) observe in 3D the impact of syn-kinematic erosion and sedimentation on a decoupled sub Andean system analogue and, in particular, (ii) to identify which part of the system is affected by sedimentation or erosion.

5.1. Role of external syn-kinematic factors (erosion/sedimentation)

We have seen that syn-kinematic sedimentation has a strong impact on the development of shallow structures, which rise when sedimentation increases, but doesn't influence depth structures significantly, especially the wavelength of deformation of deep systems are not influenced by the sedimentation.

As previously stated (Driehaus et al., 2015) the initial mechanical stratigraphy is the fundamental controlling factor. Fish tail like structures cannot develop without an interbedded decollement level, within the pretectonic pile. This prerequisite is modulated first by the sedimentation. In the absence of synkinematic sedimentary loading, the fish tail only develops for small shortening rates, as it results in a decrease of the ductile layer viscous resistance and thus in an increase of the decoupling efficiency (Couzens-Schultz et al., 2003). Intermediate sedimentation rate (E roughly of the order of ½ to 1) allows for the development of the upright, tightened fold comparable to the Incahuasi target geometry. In such case, vergence

changes occur related to the fishtail propagation and related to asymmetric decoupling (figure 7). For high sedimentation rate, the influence of the deep decoupling levels is hidden, and a more general symmetrical structure is developed, concealing the deep complexity.

Considering the impact of an uneven sedimentation, the models show that a contrast between hinterland and foreland has strong consequences: the foreland sedimentation is necessary to initiate the fold tightening, by preventing the classic foreland ward propagation of the frontal ramp. On the contrary, the hinterland sedimentation simply helps to propagate the foreland ward main thrust, by increasing the overall resistance of the moving sedimentary pile at the rear.

However, these considerations are derived from 2D, cylindrical models. Here the experiments were performed in 3D and point out to a potential modulation of these conclusions due to the lateral, along strike modifications of the sedimentation and erosion rates. The figure 15 illustrates the link between the elevation of the main deep structure (figure 15B) and the basal ductile layer thickness (figure 15C): the Northern side of the lower structure is more elevated than its counterpart to the south of the model. The basal layer thickness is also more important in the northern part of the model at the end of the shortening phase. This contrast between northern and southern part increases with shortening and results from the sedimentation ratio contrast, which vary from R=½ to R=1 (respectively from northern to southern part). The difference in sediment's weigh is responsible for a partial expulsion of the basal ductile material from the southern domain (high sediment loading) to the northern domain (low sediment loading). It thus helps amplifying the decoupling between the deep structure along the decollement surface. However, although the depth structure wavelengths are not impacted by this flowage of silicon due to variation of sedimentation rate, it appears that it helps building more symmetrical box folds, as shown by the increase in both width of the folds, and flow of silicon in the fold core.

As shown, the sedimentation (i) directly impacts shallow structures in the multi-decollement configuration, involving a vergence variation and/or tightened structures, and (ii) indirectly impacts depth structures if decollement levels are as ductile as salt or shale. But it seems that the structural style at depth is not compacted by the sedimentation rate and distribution. In contrast, we have shown that syn-kinematic erosion has a small impact on the upper structures, apart from their disappearance, but largely modifies the deeper fishtail structures: increased erosion favours an enlargement of the uppermost fold, with a progressive upward migration of the kink fold limiting the anticline limbs at depth, and thus promoting the rise of the deep fishtail. Contrarily to the case of simple sedimentation, when considering both erosion of the upper structure and sedimentation on both sides, the higher is the sedimentation, the less is developed the fishtail, as its development is precluded by its ascent in the core of the fold.

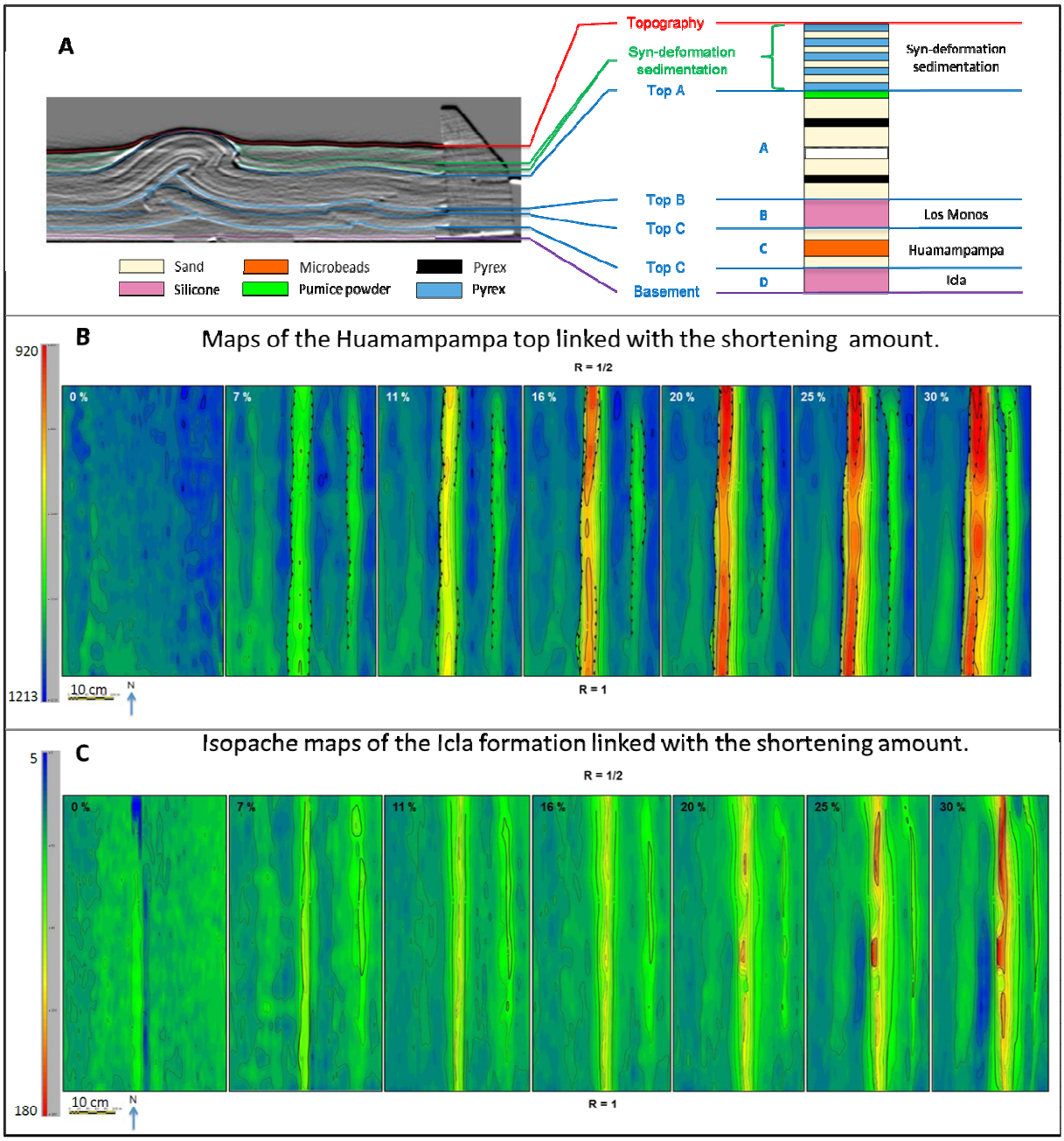

Figure 15: A. Result of the analogue model experiment testing the influence of the sedimentation. Main horizons are highlighted and correlated to the stratigraphy used. **B**. Maps of the "Huamampampa" equivalent top linked with the shortening rate. R ratio vary from 1 in the South side to ½ in the North side. Hot colors show high elevations, while cold colors show low elevations. C. Isopach maps of the "Icla" equivalentlinked with the shortening rate. R ratio vary from 1 in the South side to ½ in the North side. Hot colors show thick thickness, while cold colors show thin thickness.

5.2. Implication for petroleum exploration

Seismic imaging in foreland fold and thrust belt remains nowadays a challenge, and often only the syncline geometry are properly characterized. But structural complexity in the fold

492 core is generally high, particularly if considering pretectonic sedimentary piles implying
493 successive decollement level such as in Bolivia. It is therefore crucial for petroleum
494 exploration to know and understand the mechanisms able to trigger the decoupling, and
495 particularly to better constrain the deeper part geometry and the associated kinematic. This
496 study highlights that external factors (sedimentation and erosion) have an important impact on
497 the decoupling of superimposed structures implying variable offset of the structural
498 culminations, both in cross section and along strike of the structure. The analogue models
499 offer therefore useful guides for structural interpretation but we have shown that it is crucial
500 to constrain the natural sediment/erosion rates variations in 3D Surface data of
501 erosion/sedimentation may then provide a qualitative guide for a better assessment of deep
502 seated structure. and through time.
503
504
505 ## 6. Conclusions
506 A set of experiments have been performed to study, in 3D, the effects of external factors
507 (sedimentation and erosion) on a folded multi-decollement levels model, analogue to the fold
508 developed in the Subandean belt of Bolivia. For this case, two superimposed structures are
509 created by compression and separated by ductile decollement layers. Two structures partly
510 decoupled are formed: a deep fishtail like structures, situated below a more classic fold built
511 on a flat-ramp geometry. The role of the external forcing factors are the following:
512 (i) Sedimentation directly impacts the geometrical evolution of the shallow structures:
513 their elevation is increased and the vergences are modified when the sedimentation
514 rate is intermediate. Low sedimentation rates do not impact the foreland ward
515 propagation of the folded structure, and high sedimentation rates favour the
516 development of symmetrical pop-up.

(ii) Erosion directly impacts the evolution of deeper structures. High erosion rate, relative to the rate of the tectonic relief creation, favors the rise of these objects in the core of the upper folded structure..

The observation of these phenomenons in 3D brings new elements for the understanding of rheologically layered folded sequence. We show that despite the rough cylindrical aspect of the map view, external factors can generate misfits between the deep and shallow structural culminations. In petroleum exploration of such areas (Bolivia, Zagros,...) it is thus crucial to assess as precisely as possible syn-kinematic sedimentation and erosion rate to interpret seismic profiles and/or to built geological section, that will integrate uncertainties on the possible position of deep seated objectives. To do that, a multidisciplinary study involving (i) classical structural and sedimentological studies to understand the geodynamic of the considered system, and (ii) a dating campaign in the aim to know as much as possible the timing of syn-kinematic sedimentation and erosion and the associated ratesis mandatory.

5. Acknowledgements

Thanks to Elisabeth Rosenberg and Marie-Claude Lynch for their help in scanner analyze. Thanks to Thierry Nalpas for his help and discussion about the modeling. Many thanks to Jean Letouzey and Bernard Colletta for fruitfull discussions about worldwide examples of fold and thrust belts.

6. References

Baby P., Guillier B., Oller J., Herail G., Montemurro G., Zubieta D., Specht M., 1993. Structural synthesis of the Bolivian Sub-Andean zone. International Symposium on Andean Geodynamics, ORSTOM, Série "Colloques et Séminaires", pp. 159-162.

542 Baby P., Colletta B., Zubieta D., 1995. Etude géométrique et expérimentale d'un bassin
543 transporté : exemple du synclinorium de l'Alto Beni (Andes centrales). *Bulletin de la Société*
544 *géologique de France 166*, 797-811.

545 Barrier L., Nalpas T., Gapais D., Proust J.N., Casas A., Bourquin s., 2002. Influence of
546 syntectonic sedimentation on thrust geometry. Field examples from the Iberian Chain (Spain)
547 and analogue modeling. *Sedimentary Geology 146*, 91-104.

548 Barrier L., Nalpas T., Gapais D., Proust J-N., 2013. Impact of synkinematic sedimentation on
549 the geometry and dynamics of compressive growth structures: Insights from analogue
550 modelling. Tectonophysics, 16p.

551 Bonini M., 2001. Passif roof thrusting and forelandward fold propagation in scaled brittle-
552 ductile physical models of thrust wedges. *Journal of Geophysical Research 106*, 2291-2311.

553 Buttler R., Richards D., Sempere T., Marshall L., 1995. Paleomagneti determinations of
554 vertical-axis rotations from Late Cretaceous and Paleocene strata of Bolivia. *Geology 23*, 799-
555 802.

556 Callot, J.P., J Letouzey, S. Jahani, S. Sherkati, 2012. Pre-existing salt structures and the
557 folding of the Zagros Mountain. From: Alsop, G. I., Archer, S. G., Hartley, A. J., Grant, N. T.
558 & Hodgkinson, R. (eds) 2012. Salt Tectonics, Sediments and Prospectivity, Geological
559 Society, London, Special Publications, 363, 545–561. http://dx.doi.org/10.1144/SP363.27

560 Casas A.M., Gapais D., Nalpas T., Besnard K., Roman Berdiel T., 2001. Analogue models of
561 transpressive systems. *Journal of Structural Geology* 23, 733-743.

562 Chemenda AI, Burg JP, Mattauer M. 2000. Evolutionary model of the Himalaya-Tibet
563 system: geopoembased on new modelling, geological and geophysical data. Earth and
564 Planetary Science Letters 174:397-409

565 Cobbold P.R., Davy P., Gapais D., Rossello E.A., Sadybakasov E., Thomas J.C., Tondji Biyo
566 J.J., de Urreiztieta M., 1993. Sedimentary basins and crustal thickening. *Sedimentary Geology*
567 86, 77-89.

568 Cobbold, P.R., Clarke, B.J., Løseth, H., 2009. Structural consequences of fluid overpressure
569 and seepage forces in the outer thrust belt of the Niger Delta. Petroleum Geoscience 15, 3-15.

570 Colletta B., Letouzey J., Pinedo R., Ballard J. F., Bale P., 1991. Computerized X-ray
571 tomography analysis of sand box models: examples of thin-skinned thrust system: *Geology*
572 *19*, 1063-1067.

573 Colletta B., Letouzey J., Soares J., Specht M., 1999. Detachment versus fault-propagation
574 folding: Insights from the Sub-Andean Ranges of southern Bolivia. *Thrust Tectonics*
575 *Conference, Royal Holloway, University of London, Abstracts,* 106-109.

576 Diraison M., Cobbold P. R., Gapais D., Rossello E.A., Le Corre C., 2000. Cenozoic crustal
577 thickening, wrenching and rifting in the foothills of the southernmost Andes. Tectonophysics
578 316, 91-119.

579 Driehaus L., Nalpas T., Ballard J. F., 2014. Interaction between deformation and
580 sedimentation in a multidecollement thrust zone: Analogue modelling and application to the
581 Sub-Andean thrust belt of Bolivia. Journal of Structural Geology 65, 59-68.

582 Gestain V., Nalpas T., Rouby D., Barrier L., 2004. Rôle des niveaux incompétents
583 syncinématiques sur l'évolution des structures chevauchantes. *Bulletin de la Société*
584 *Géologique de France 175*, 351-359.

585 Gubbels T.L., Isacks B.L., Farrar E., 1993. High-level surfaces, plateau uplift, and foreland
586 development, Bolivian central Andes. *Geology 21*, 695-698.

587 Hardy S., Duncan C., Masek J., Brown D., 1998. Minimum work, fault activity and the
588 growth of critical wedges in fold and thrust belts. *Basin Research 10*, 365-373.

589 Hounsfield G. N., 1973. Computerized transverse axial scanning (tomography). *British J.*
590 *Rad. 46*, 1016-1022.

591 Hubbert M. K., 1937. Theory of scale models as applied to the study of geologic structures.
592 *Geological Society of America 48*, 1459-1520.

593 Johnson M.R.W., 1981. The erosion factor in the emplacement of the keystone thrust sheet
594 (South East Nevada) across a land surface. *Geological Magazine 118*, 501-507.

595 Koyi H.A., Hessami K., Teixell A., 2000. Epicenter distribution and magnitude of
596 earthquakes in fold-thrust belts: Insights from sandbox models. *Geophysical Research Letters*
597 *27*, 237-276.

598 Labaume P., Simon M. F. Sheppard, Moretti, I., 2001. Fluid flow in cataclastic thrust fault
599 zones in sandstones, Sub-Andean Zone, Southern Bolivia. *Tectonophysics 340*, 141-172.

600 Lebel D., Langenberg W., Mountjoy E. W., 1996. Structure of the Central Canadian
601 Cordilleran Thrust-and-Fold Belt, Athabasca-Brazeau Area, Alberta: A Large, Complex
602 Intercutaneous Wedge. Bulletin of Canadian Petroleum Geology, Vol 44, N°2, p. 282-298.

603 Letouzey J., Colletta B., Vially R., Chermette J. C., 1995. Evolution of salt-related structures
604 in compressional settings. Salt tectonics: a global perspective. *American Association of*
605 *Petroleum Geologists Memoir*, 65, 41-60.

606 Leturmy P., Mugnier J.L., Vinour P., Baby P., Coletta B., Chabron E., 2000. Piggyback basin
607 development above a thin-skinned thrust belt with two detachments levels as a fonction of
608 interactions between tectonic and superficial mass transfer: the case of the Subandean Zone
609 (Bolivia). Tectonophysics 320, 45-67.

610 Liu H., McClay K.R., Powell D., 1992. Physical models of thrust wedges. *Thrust tectonics*.
611 McClay K. R. (ed), Chapman & Hall, London, 71-81

612 Malavieille J., Larroque C., Calassou S., 1993. Experimental modelling of
613 tectonic/sedimentation relationships between forearc basin and accretionary wedge. *Comptes*
614 *Rendus de l'Académie des Sciences de Paris, Série IIa*, 316, 1131-1137.

615 Mandl G., 1988. Mechanisms of Tectonic Faulting. *Elsevier, Amsterdam*.

616 Marshall L., Sempere T., Gayet M., 1993. The Petaca (Late Oligocene – Middle Miocene)
617 and Yecua (Late Miocene) formations of the Sub-Andean Chaco Basin, Bolivia, and their
618 tectonic significance. *Documents des Laboratoires de Geologie de la Faculté des Sciences de*
619 *Lyon 125*, 291-301.

620 Merle O., Abidi N., 1995. Approche expérimentale du fonctionnement des rampes
621 émergeantes. *Bulletin de la Société Géologique de France 166*, 439-450.

622 Moretti I., Baby P., Mendez E., Zubieta D., 1996. Hydrocarbon generation in relation to
623 thrusting in the Sub Andean Zone from 18 to 22°S, Bolivia. *Petroleum Geosciences 2*, 17-28.

624 Moretti I., Labaume P., Sheppard S. M.F., Boulègue J., 2002. Compartmentalisation of fluid
625 migration pathways in the sub-Andean Zone, Bolivia. *Tectonophysics 348*, 5-24.

626 Mugnier J.L., Baby P., Coletta B., Vinour P., Balé P., Leturmy P., 1997. Thrust geometry
627 controlled by erosion and sedimentation: a view from analogue models. *Geology 25*: 427-430.

628 Nalpas T., Györfi I., Guillocheau F., Lafont F., Homewood P., 1999. Influence de la charge
629 sédimentaire sur le développement d'anticlinaux synsédimentaires. Modélisation analogique
630 et exemples de terrain (Bordure sud du bassin de Jaca). *Bulletin de la Société Géologique de*
631 *France 170*, 733-740.

632 Nalpas T., Gapais D., Verges J., Barrier L., Gestain G., Leroux G., Rouby D., Kermarrec J.J.,
633 2003. Effects of rate and nature of synkinematic sedimentation on the growth of compressive
634 structures constrained by analogue models and field examples. *Geological Society of London*
635 *Special Publication 208*, 307-319.

636 Nieuwland D.A., Leutsher J.H., Gast J., 2000. Wedge equilibrium in fold-and-thrust belts:
637 prediction of out-of-sequence thrusting based on sandbox experiments and natural examples.
638 *Geologie en Mijnbouw 79*, 81-91.

639 Pichot T., Nalpas T., 2009. Influence of synkinematic seimentation in a thrust system with
640 two decollement levels; analogue modelling. *Tectonophysics 473*, 466-475.

641 Price N.J., Johnson M.R.W., 1982. A mechanical analysis of the Keystone-Muddy mountain
642 thrust sheet in the southeast Nevada. *Tectonophysics 84*, 131-150

643 Raleigh C.B., Griggs D.T., 1963. Effect of the toe in the mechanics of overthrust faulting.
644 *Geological Society of America Bulletin*, 74: 819-830

645 Ramberg H., 1981. Gravity, deformation and the Earth's crust. *Academic Press, New York.*

Richard P., Cobbold P. R., 1989. Structures en fleur positives et décrochements crustaux: modélisation analogique et interprétation mécanique. *Compte rendu de l'Académie des Sciences de Paris 308,* 553-560.

Schreurs G., Buiter S. J. H., Boutelier D., Corti G., Costa E., Cruden A. R., Daniel J. M., Hoth S., Koyi H. A., Kukowski N., Lohrmann J., Ravaglia A., Schlische R. W., Withjack M. O., Yamada Y., Cavozzi C., Delventisette C., Elder Brady J. A., Hoffmann-Rothe A., Mengus J.-M., Montanari D., Nilforoushan F., 2006. Analalogue benchmarks of shortening and extension experiments. *Geological Society, London, Special Publications 253,* 1-27.

Sempere T., Carlier G., Carlotto V., Jacay J., Jimenez N., Rosana S., Soler P., Cardenas J., Boudesseul N., 1999. Late Permian-Early Mesozoic rifts in Peru and Bolivia, and their bearing on Andean-age tectonics. Fourth ISAG, Goettingen (Germany), Abstracts Volume, pp. 680-685.

Couzens-Schultz B., Vendeville B., Wiltschko D., 2003. Duplex style and triangle zone formation: insights from physical modeling. Journal of Structural Geology 25, 1623-1644.

Soler P., Sempere T., 1993. Stratigraphie, géochimie et signification paléotectonique des roches volcaniques basiques mésozoïques des Andes Boliviennes. *Comptes Rendus de l'Académie des Sciences, Paris, Série II 316,* 777-784.

Storti F. et McClay K., 1995. Influence of syntectonic sedimentation on thrust wedges in analogue models. *Geology 23,* 999-1002.

Storti F., Salvini F., McClay K., 2000. Synchronous and velocity-partitioned thrusting and thrust polarity reversal in experimentally produced, doubly-vergent thrust wedges: implication for natural orogend. *Tectonics 19,* 378-396.

668 Tondji Biyo J.J., 1995. Chevauchements et bassins compressifs: influence de l'érosion et de la
669 sédimentation. *Thèse de doctorat de l'Université de Rennes I*, 406pp.

670 Twiss R.J., Moores E. M., 1992. Structural Geology. *Freeman, New-York*, 532p.

671 Uba, C.E., Heubeck, C., Hulka, C., 2005. Facies analysis and basin architecture of the
672 Neogene Subandean synorogenic wedge, southern Bolivia. Sedimentary Geology 180, 91-
673 123. doi: 10.1016/j.sedgeo.2005.06.013.

674 Uba, C.E., Heubeck, C., Hulka, C., 2006,.Evolution of the late Cenozoic Chaco foreland 516
675 basin, southern Bolivia. Basin Research 18, 145-170, doi: 10.1111/j.1365-2117.2006.00291.x.

676 Verges, J., Goodarzi, M. G. H., Emami, H., Karpuz, R., Efstathiou, J., Gillespie, P., 2011.
677 Multiple detachment folding in Pusht-e Kuh arc, Zagros: Role of mechanical stratigraphy. In:
678 McClay, K., Shaw, J., Suppe, J. (Eds.), Thrust fault-related folding: AAPG Memoir 94, 69-
679 94.

680 Vidal-Royo O., Hardy S., Munoz J. A., 2011. The roles of complex mechanical stratigraphy
681 and syn-kinematic sedimentation in fold development: insights from discrete-element
682 modelling and application to the Pico del Aguila anticline (External Sierras, Southern
683 Pyrenees). Geological Society of London, Special Publication 349, 45-60.